Structural Characterization of Phosphate Species Adsorbed on γ-Alumina by Combining DNP Surface Enhanced NMR Spectroscopy and DFT Calculations

Adrian Hühn, Dorothea Wisser, Manuel Corral Valero, Teddy Roy, Mickaël Rivallan, Leonor Catita, Anne Lesage, Carine Michel, Pascal Raybaud

Structural Characterization of Phosphate Species Adsorbed on γ-Alumina by Combining DNP Surface Enhanced NMR Spectroscopy and DFT Calculations

Adrian Hühn,[§] Dorothea Wisser,[†a] Manuel Corral Valero,[†] Teddy Roy,[†] Mickaël Rivallan,[†] Leonor Catita,[†] Anne Lesage,[‡]* Carine Michel,[§]* and Pascal Raybaud[†§]*

† IFP Energies nouvelles, Rond-point de l'échangeur de Solaize, Solaize BP 3, 69360, France.

[§]Univ Lyon, ENS de Lyon, CNRS UMR 5182, Laboratoire de Chimie, Lyon F69342, France.

[‡]Centre de RMN à Très Hauts Champs, Université de Lyon (CNRS/ENS Lyon/UCB Lyon 1), Villeurbanne 69100, France.

[a]current address: Erlangen Center for Interface Research and Catalysis, Friedrich-Alexander-Universität Erlangen-Nürnberg, Egerlandstraße 3, 91058 Erlangen, Germany

KEYWORDS : γ–alumina, Phosphate, Polyphosphate, Density functional theory, chemical shift, Nuclear magnetic resonance spectroscopy, DNP SENS

ABSTRACT

Obtaining an atomic-scale description of the chemical interactions of phosphates with an oxide support, such as γ-Al_2O_3 is essential to get a rational understanding of the role of phosphate additives for a great number of heterogeneous catalysts, as well as to improve the use of this element. Combining cutting-edge Dynamic Nuclear Polarization Surface Enhanced NMR Spectroscopy (DNP SENS) techniques with Density Functional Theory (DFT) calculations, we provide an accurate molecular description of phosphate speciation on γ-Al_2O_3 surfaces for various P surface coverages after drying at 120°C. Thanks to ^{31}P double- and triple-quantum filtered NMR experiments as well as to ^{27}Al-^{31}P dipolar- and scalar-based correlation spectra, we demonstrate the presence of polyphosphates and of Al-O-P connectivities at the exposed facets of γ-Al_2O_3. DFT-based thermodynamics shows that phosphates (mono- or di-) are preferentially covalently bonded on the (1 1 0) γ-Al_2O_3 facet with high-dentation modes. These high-dentation modes are favored by entropy gain due to water desorption. We used the gauge-including projector-augmented wave (GIPAW) DFT method for ^{31}P NMR chemical shifts calculations and propose a systematic identification of the various types of phosphates covalently or non-covalently bonded to the alumina surface. The calculations confirm the existence of polyphosphates as observed experimentally. Since the surface condensation into polyphosphates is endergonic, the presence of polyphosphates on the surface is likely to result from their direct adsorption in impregnation solution. The observed increasing concentration of polyphosphates with the coverage could be related to a less-likely hydrolysis due to the reduced availability of sites to stabilize the fragmented oligomers. This understanding opens the road to

a better control over the speciation of phosphate species that are known to be key in the preparation of supported catalysts over alumina.

1. INTRODUCTION

The use of organic or inorganic additives is central in the nowadays preparation of heterogeneous catalysts from the laboratory to the industrial scale. In particular, phosphates are widely used class of inorganic additives which contributes to the continuous improvement of performances of a large number of industrial heterogeneous supported catalysts,[1–4] although many questions are still raised on its molecular interplay with the support and the active phase. Considering first the case of MoS_2 based hydrodesulfurization catalysts, adding phosphoric acid during the preparation steps (impregnation) increases the catalytic rates, although this effect depends closely on the P surface concentration.[4,5] The presence of phosphate species on alumina was proposed to decrease the Mo oxide/alumina interaction[6], to tune the nature of oxide precursor[7] and to enhance the sulfo-reduction of Mo oxide precursor[5] by tuning its interaction with surface phosphates.[8] It was further proposed that the presence of P on the support may also directly impact the architecture of the MoS_2 active phase through direct P-O-Mo bridge or direct replacement of sulfide species by phosphorus.[9] In addition, phosphorus containing impregnation solution modifies the interplay between the various solvated metal ions and their interactions with the alumina support,[1,4] in order to avoid the formation of undesirable and inactive phases,[2,10,11] and impact the genesis of the MoS_2 active phase itself.[12] In particular, Garcia de Castro et al. showed that the dispersion state of phosphate depends on the surface exposed by alumina particles, which in turn influences the sulfidation rate and the growth of MoS_2 active phase.[12]

In the case of Fischer-Tropsch cobalt catalysts, it was proposed that the pre-impregnation of phosphoric acid on alumina enhance the reducibility of the cobalt oxide precursor the stability of the supported catalyst in presence of water.[13,14] This trend was interpreted as a specific interaction of cobalt with phosphate species deposited on alumina surfaces which prevents the aggregation of cobalt particles. Similarly, for biomass conversion reaction in liquid phase,

adding phosphorus on alumina increases its hydrothermal stability, limiting its transition to boehmite,[3] and prevents the metallic phase from leaching.[15] In the various works cited before, the P loading was allowed to vary between 0.5 and 10 wt% which may lead to a great diversity of phosphate species (including $AlPO_4$) depending on the preparation method, the P loading, and the thermal treatment.[7,16] This work showed the complexity of P surface speciation but also its importance, as one should expect that the catalytic effects of those P species differ. However, although it is accepted that at high loadings the catalytically undesirable $AlPO_4$ phase forms, little is known about the catalytic trends induced by the presence of phosphate monomers, dimers, trimers and oligomers in alumina surfaces. Hence, providing a molecular scale description of the surface P speciation prior $AlPO_4$ formation, is key for a better rational understanding of its impacts on the various properties of supported heterogeneous catalysts.

Several analytical approaches, such as spatially-resolved Raman and UV-visible-NIR spectroscopy,[17] X-ray absorption spectroscopy, [11,18] or Raman imaging techniques [19] have been applied in order to describe the phosphate species adsorbed onto alumina and elucidate their role in the different stages of catalysts preparation. Infrared (IR) spectroscopy on samples, either dried or in solution, has also been used to investigate the adsorption of phosphates onto γ-alumina, and successfully demonstrated the presence of interactions between γ-Al_2O_3 carriers and phosphate anions.[20–22] IR revealed also the evolution of the vibrational frequency of alumina OH groups as a function of phosphates concentration and provided interesting insights into the nature of OH groups involved in the exchange mechanisms in various conditions.[7,8,23,24] However, an unambiguous identification of the adsorption mode of phosphates by IR spectroscopy remains difficult, as the vibrational frequencies of adsorbed phosphates cannot be easily deconvoluted.[23] Hence, direct insight into the local P environment at the atomic scale required the use of alternative approach.

Nuclear Magnetic Resonance (NMR) is in principle a method of choice to get an atomic-scale characterization of phosphates in interaction with alumina, and indeed several NMR studies have been reported that tentatively describe those complex structures.[25,26] Notably, in 1991, DeCanio et al. recorded one-dimensional (1D) ^{31}P NMR spectra of a series of catalytic Al_2O_3 materials, where the phosphorus loading of the catalyst was varied from 0.5 to 10 wt %,[7] which, jointly with XRD data, suggested the presence of monomeric and polymeric phosphate species, as well as of both amorphous and crystalline aluminum phosphate at high phosphorus loadings. A few years later, van Eck et al. implemented 1D $^{31}P\{^{27}Al\}$ REDOR and TRAPDOR experiments on phosphorus-impregnated γ-Al_2O_3, to probe proximities between phosphorus and aluminum atoms.[27] The formation of a layer of aluminum phosphate on alumina was observed at a phosphorus loading of 2 wt %, while the existence of bulk phosphate layers was excluded, even at higher loading. More recently, Phillips and co-workers applied 1D REAPDOR experiments and DFT simulations to probe the dentation mode of phosphates adsorbed at the water-boehmite [28] and water-corundum [22] interfaces. The experimental results, interpreted jointly with DFT calculations and IR data, point towards the existence of bidentate binuclear surface complexes as the dominant species. The intrinsic low sensitivity of NMR, combined with the low content of phosphorus species (a few percent in weight of the total sample or even less) has so far prevented the implementation of NMR approaches, including two-dimensional techniques, that would provide additional structural details on the various phosphate species at the surface of alumina.

Dynamic Nuclear Polarization Surface Enhanced NMR Spectroscopy (DNP SENS) has recently been developed as a unique technique to probe the atomic-scale structure of surface species in catalytic materials.[29–32] In this approach, an exogeneous polarizing agent, usually a biradical, is added to the sample, and the huge polarization of the unpaired electrons is transferred to the neighbouring protons by microwave irradiation. As a result, the NMR signals

are enhanced by typically two orders of magnitude. This corresponds to drastic reduction in experimental time (by typically four orders of magnitude), enabling the fast acquisition of multiple-pulse and/or multi-nuclear experiments, including on dilute surface species that are difficult to characterize in a comprehensive way using conventional NMR approaches.

Simultaneously, progresses in computational chemistry, including DFT based approaches, enable today the implementation of coherent strategies to understand and describe at the atomic-level some crucial steps, such as impregnation, drying or activation, involved in the preparation of supported heterogeneous catalysts.[33] The atomistic models of γ-Al_2O_3 surfaces determined in ref. [34,35] were used to simulate the interaction cobalt hydroxide catalytic precursors[36] and oxygenated organic additive molecules used in catalytic preparation.[37] In parallel, thanks to progress in the theoretical determination of NMR chemical shifts for periodic systems using the gauge-including projector-augmented wave (GIPAW) method,[38,39] an advanced interpretation of the NMR spectroscopic features can now be proposed that guides their assignment to specific bulk or surface sites. Regarding the alumina supports, the combination of DNP SENS and DFT calculations made possible to unravel the nature of surface Brønsted acid sites.[40,41] Moreover, several recent theoretical studies were reported on the calculations of ^{31}P NMR chemical shifts inside various bulk materials that provide an accurate assignment of the various phosphorus sites inside bulk aluminum phosphates.[28,42–46]

The key questions related to the role of phosphorus (as phosphate species) in catalytic applications concern the precise nature of its interaction with the alumina supports and with the metallic precursors of the active phase. Answering this general question would require not only to investigate the effect of phosphorus/metallic precursor content but also the effect of thermal treatment of the surface. By using a heuristic approach, we propose to focus here on the speciation of phosphorus on alumina under drying conditions and for relevant phosphorus contents, conditions which are at the crossing road of the synthesis of numerous catalytic

systems cited before. Addressing the questions related to the oligomerization degree of phosphates, to their dentation modes and to the alumina surface sites involved in the anchoring, will help to better understand how phosphorus may impact at a molecular scale, the deposition of the metallic active phase of the catalyst.

For this purpose, we combine DNP SENS on a series of γ-Al_2O_3 samples impregnated with phosphoric acid and DFT calculations to identify the localization, adsorption mode and speciation of phosphorus on γ-Al_2O_3. The coverage is expected to play a key role in those aspects, and we have chosen to study a concentration range in phosphoric acid from 0.4 to 4.45 wt% (i.e.: 0.4 to 4.1 P nm^{-2} according to the surface area of our alumina samples).

We first present the results related to the NMR investigations. Notably, the sensitivity gain provided by DNP allows one to directly detect oligomeric phosphates via the implementation of ^{31}P multiple-quantum filtered NMR experiments, as well as to record two-dimensional (2D) ^{27}Al-^{31}P correlation spectra, which provides new insights into the adsorption mode. Then, we present the results related to our *in silico* screening of all possible adsorption modes of phosphoric acid on the two most exposed alumina facets ((1 0 0) and (1 1 0)), including co-adsorption and dimer adsorption. Lastly, we provide in discussion a refined interpretation of the NMR experiments based on the computed ^{31}P NMR isotropic chemical shift of the most relevant structures and the possible implications for the catalytic active phase.

2. RESULTS

Most of the scientific literature in catalysis recalled in Introduction quantify the adsorption of phosphorus species on oxide carriers between 0.5 and 10 %wt P. As explained before, according to previous experimental works,[7,8,23] the $AlPO_4$ phase may appear at concentrations above 4.5 wt % P. Since this phase is strongly suspected to be detrimental to the catalytic performances, our samples will explore P loadings below this threshold (from 0.4 to 4.3 wt% P) and after

applying a moderate thermal treatment (drying at 120°C, and ambient pressure overnight) avoiding the diffusion of P into alumina bulk. In order to provide a molecular view of the phenomena in line with NMR characterization and DFT simulations, we will express our results in terms of surface concentrations (that is, P atoms per unit surface). For experimental samples, it turns out that experimental surface concentrations of 1 P nm^{-2} is roughly equivalent to 1 % wt P in our samples (with specific surface area of 209 m^2 g^{-1} of Pural SB3). Hence, our samples will explore surface concentration of 0.5 to 4.1 at nm^{-2} (see also **Supporting Information S1.1** for more details on samples preparations).

2.1. **NMR experiments**

In a first step, we aimed at probing all possible phosphate species present on the γ-Al2O3 surface. One-dimensional (1D) room temperature ^{31}P cross-polarization (CP) Magic Angle Spinning (MAS) NMR spectra were recorded (**fig. 1a**) on the series of γ-Al_2O_3 (Pural SB3) samples described before. Details on the NMR experiments are reported in **Supporting Information S1.2**. We note that CP experiments transfer polarization from protons to nearby ^{31}P nuclei, and consequently, do not yield quantitative spectra. As observed previously by DeCanio *et al*,[7] the ^{31}P spectra exhibit a broad resonance, the maximum of which shifts to lower chemical shift values with increasing concentration of amount of adsorbed phosphates, measured by X-ray fluorescence spectroscopy (from -5.8 ppm at 0.4 P nm^{-2} to -16.1 ppm at 4.1 P nm^{-2}). At low phosphate coverage the resonance spans between 0 and -20 ppm, while at higher coverage, the distribution of chemical shifts spreads up to -30 ppm. These broad resonances likely correspond to overlapping contributions arising from various phosphate species that cannot be discerned at this stage. One-dimensional ^{31}P direct excitation spectra were also recorded in order to probe the presence of a crystalline aluminum phosphate phase, which is expected to exhibit a characteristic narrow NMR signal at around -32 ppm.[7] We did not see

this signal and we thus excluded the formation of such a phase at the low coverage rates investigated here.

More advanced one- and two-dimensional experiments were then implemented to gain additional insights into the possible structural motifs of the phosphate species. These experiments were carried out under Dynamic Nuclear Polarization (DNP) to enhance the sensitivity of NMR spectra and enable the acquisition of the data in reasonable experimental times.

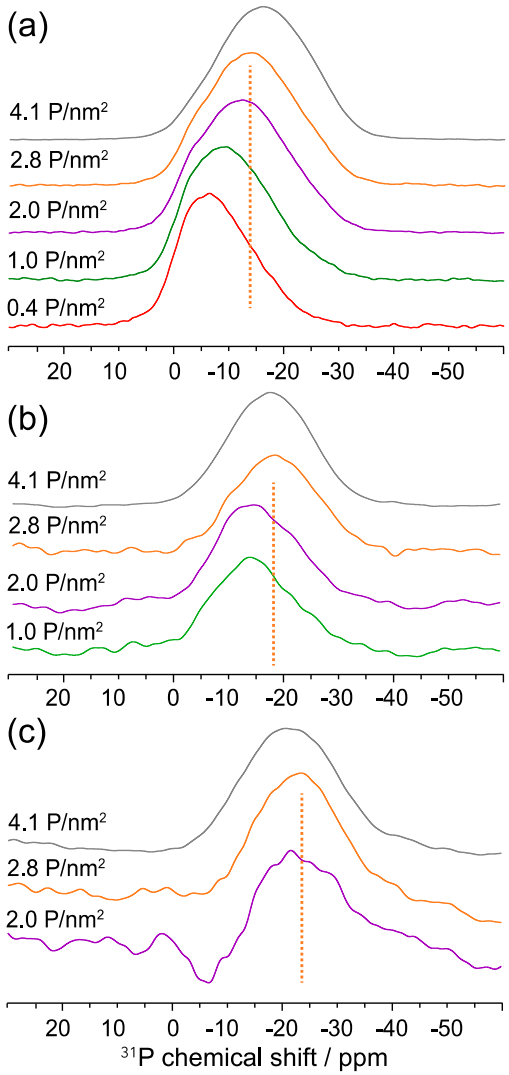

Figure 1. (a) One-dimensional ^{31}P CP MAS spectra of phosphate species adsorbed on γ-Al_2O_3 for various surface coverages. The spectra were recorded at 9.4 T (400 MHz ^{1}H resonance frequency), in a 2.5 mm zirconia rotor at a MAS rate of 30 kHz and at room temperature. (b) One-dimensional DNP-enhanced ^{31}P MAS refocused-INADEQUATE spectra of phosphate

species adsorbed on γ-Al_2O_3 for various surface coverages. (c) One-dimensional DNP-enhanced ^{31}P MAS through-bond triple-quantum filtered spectra. All the DNP NMR spectra were recorded at 9.4 T (400 MHz ^{1}H resonance frequency, 263 GHz microwave frequency) in 3.2 mm sapphire rotors at a MAS frequency of 8 kHz and a sample temperature of around 110 K. Other experimental details are given in the SI. The orange dotted line illustrates the high-field shift in frequencies observed from the single- to the double- and triple-quantum filtered experiments for the 2.8 P/nm^2 surface coverage. Spectral intensities were normalized. An exponential line broadening of 500 Hz was applied to all spectra.

For the DNP experiments, the samples were impregnated with a solution of 16 mM TEKPol [47] in 1,1,2,2-tetrachloroethane (TCE) via the incipient wetness method, as described in the **Supporting Information 1.1**. Solvent enhancement factors between 95 and 132, and surface enhancement factors between 98 and 113, determined from ^{31}P CPMAS spectra, were obtained (**Table S2).**

In order to probe the possible presence of bi- or longer polyphosphates on the surface as proposed by previous studies, [7,16] we first carried out experiments that rely on through-bond ^{31}P-^{31}P interactions to filter the NMR signal of phosphorus atoms involved in *J*-coupled spin pairs or triplets, and thus to assess the presence of biphosphates and higher polyphosphates in the materials. **Fig. 1b** shows 1D ^{31}P MAS refocused INADEQUATE [48,49] spectra recorded on the series of samples. This experiment allows the determination of spin-spin connectivities through the creation of homonuclear double-quantum (DQ) coherences. A ^{31}P DQ-filtered INADEQUATE signal could be observed for all the γ-Al_2O_3 samples with a phosphorus coverage higher than 1.0 P nm^{-2}, which demonstrates unambiguously the presence of P-O-P species, i.e. of di- or higher polyphosphates. The resonance corresponds to a broad distribution between 0 and -30 ppm with a maximum at around -13 ppm for the 1 and 2 P nm^{-2} coverages, and at around -18 ppm for higher P loading. No signal could be detected for the sample with the 0.4 P nm^{-2} loading, even after 1024 scans (~ one hour of acquisition time). This indicates

that, for this coverage, polyphosphate species are absent or more likely, present but at an extremely low amount, which makes them undetectable under our experimental conditions. The relative fraction of P-O-P species was estimated from the signal-to-noise ratio per unit of time of INADEQUATE and CP experiments, and from measured values of ^{31}P transverse coherence lifetime T_2', as detailed in **Figure S1**. The data shows that the relative fraction of polyphosphates increases with increasing phosphorus loading, with a factor 3.5 difference between the lowest (1 P nm^{-2}) and highest (4.1 P nm^{-2}) surface coverage.

One-dimensional DNP enhanced through-bond triple-quantum (TQ) filtered experiments were also carried out. The pulse sequence we used was similar to that of the INADEQUATE experiments, but the phase cycling was modified to excite and reconvert TQ coherences as proposed by Fayon et al. [50] As described in this reference, for a linear three-spin system, the 1D experiment yields a signal at the resonance frequency of the central nucleus, i.e. in our case of central phosphorus atoms in tri- or longer polyphosphates. **Fig. 1c** shows 1D ^{31}P TQ-filtered spectra of γ-alumina with phosphate coverages ranging from 2.0 to 4.1 P nm^{-2}. In all cases, a signal centered at around -21 ppm is observed. This value is in line with the chemical shift reported by Yoza *et al.* for the central phosphorus atom of tri- or higher polyphosphates in solution. [51] No signal corresponding to P-O-P-O-P species could be detected for the 1.0 and 2.0 P nm^{-2} samples suggesting either the absence of such species or their presence in very small amounts. We note that tri- or higher polyphosphates will contribute to the DQ-filtered 1D spectra of **Fig. 1b,** and that the shift observed towards lower chemical shifts in these DQ spectra with increasing phosphate content could be explained by an increasing fraction of phosphate oligomers. As in the case for the 1D CP MAS spectra, single contributions can however not be resolved.

Phosphates may be bound to the alumina by covalent bonds or by weak interactions such as hydrogen bonds only, or both states may coexist. To probe these two possible states, advanced

solid-state NMR techniques have been established. Yet, they are particularly challenging in a system where phosphate is only present in small amounts. The huge sensitivity gain provided by DNP also enabled the acquisition of 2D ^{27}Al-^{31}P correlation experiments that probe either through-space proximities or as through-bond connectivities between phosphorus and surface aluminum atoms. **Figure 2** shows ^{27}Al-^{31}P scalar-based INEPT[52,53] (Insensitive Nuclei Enhanced by Polarization Transfer) spectra recorded on the series of the impregnated alumina samples. This experiment relies on two-bond Al-O-P isotropic scalar couplings to transfer the polarization from ^{31}P to ^{27}Al nuclei. The dipolar-based INEPT spectra, based on the heteronuclear dipolar interaction between the two types of spins, are shown in **Figure S2**. 1D ^{31}P projections of the through-space and through-bond correlation maps, as well as the 1D ^{31}P CPMAS spectra are reported on the left of the 2D plots in **Figure 2**. γ-Al_2O_3 exposes three types of Al sites that differ in their coordination sphere: tetra-, penta- and hexa-coordinated sites, conventionally labeled respectively as Al_{IV}, Al_V and Al_{VI}, and INEPT experiments reveal to which alumina coordination sites phosphate is close in space or covalently bound. We first observe that a large fraction of the ^{31}P chemical shift distribution correlates with all types of Al sites in the scalar-based INEPT spectra of **Figure 2** regardless the phosphorus loading. This demonstrates the formation of covalent bonds Al-O-P at each coverage rate. As shown in the 1D projections along the aluminum dimension, this covalent bonding involves mainly Al_{IV} and Al_{VI} sites. Also signals indicative for covalent bonding to Al_V are visible. The latter are less intensive, which may reflect the overall lower number of Al_V sites on the alumina surface.

The comparison of the 1D ^{31}P CPMAS spectra (in red) and of the chemical shift envelope of the phosphorus linked to aluminum (in black) indicates that part of the ^{31}P nuclei is not covalently bonded to the surface. This is especially true for phosphorus loadings between 0.4 and 2.0 P/nm^2. The comparison of the ^{27}Al projections (**fig. S3)** shows that the intensity distribution of the ^{27}Al signals differs in dipolar- and scalar-based correlation experiments,

which also supports the assumption that a fraction of the ^{31}P is not covalently attached to the surface. This would also explain the differences in the average ^{31}P and ^{27}Al chemical shifts observed for a given phosphorus loading in through-bond and through-space correlations (see the corresponding ^{31}P projections in black and blue respectively, in **Figure 2** as well as in **Figure S2**). These discrepancies agree with literature data on alumino-phosphate materials, in which up-field ^{27}Al and ^{31}P shifts are observed with respect to pure alumina samples [54] and free phosphates [51,55]. The ^{31}P resonance of phosphates covalently bound to boehmite was recently reported between 0 and -10 ppm. [22,55] The ^{31}P chemical shifts in the scalar-based INEPT experiments in this work range span a much broader range, from 0 to -30 ppm. In addition, the maximum of the chemical shift distribution shifts to lower ppm values with increasing P surface coverages (from -12 to -18 ppm). This shift comes along with a similar change in the ^{27}Al frequencies: **Tables S3 and S4** highlight a constant upfield shift of the ^{27}Al chemical shift values for the 3 sites extracted from the projections of the 2D spectra. The progressive ^{31}P shift could be explained by the contribution of polyphosphates, which exhibit lower chemical shift values at high P loading. As illustrated in **Figure S6** for the 4.1 P/nm^2 coverage, the chemical shift distribution of the polyphosphates superimposes quite well with the ^{31}P projection of the *J*-based INEPT spectrum. This would also suggest that the polyphosphates are largely chemically bond to the surface for the highest coverage.

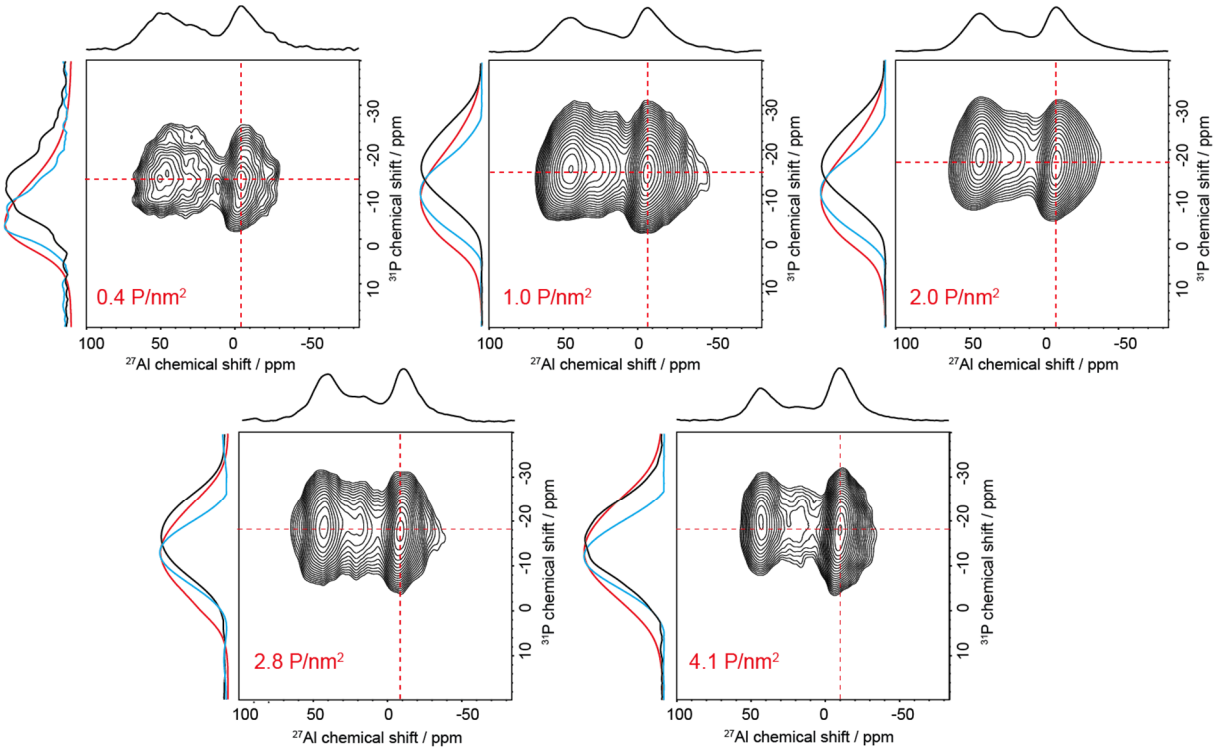

Figure 2. Two-dimensional DNP enhanced through-bond ^{31}P-^{27}Al INEPT correlation spectra recorded at 9.4 T (400 MHz ^{1}H resonance frequency, 263 GHz microwave frequency, approx. 110 K for the sample temperature). The MAS frequency was 12 kHz for the 0.4, 1 and 2 P/nm^2 loading, and 8 kHz for the others. The dotted red lines illustrate the shifts in frequency with increasing coverages. The 1D ^{31}P CP MAS spectra (red line) as well as the projections along the indirect dimension of the 2D through-bond (black line) and through-space (blue line) spectra are reported on the left of the 2D maps. The projection along the ^{27}Al dimension is shown above the plots. Other experimental details are reported in **Supporting Information 1.2**.

To summarize, DNP SENS experiments point out to the presence of multiple phosphate species. In particular, bi-, tri- and possibly higher polyphosphates were detected. The formation of biphosphate was observed in the 1.0 to 4.1 P/nm^2 range, and was shown to increase with increasing coverage rates. The formation of phosphate species covalently attached to the alumina surface was also observed at all phosphate loadings. Phosphorus atoms mainly bind to Al_{IV} and Al_{VI}, with ^{31}P and Al isotropic chemical shifts values that decrease with increasing surface coverage. A fraction of the phosphate species appears to be non-covalently attached to the surface. Despite the richness of this information, DFT calculations of the chemical shifts

are neded to refine the interpretation of the NMR spectra and provide a complete atomic-scale description of the phosphate species adsorbed at the alumina surface.

2.2. DFT computations of stability and ^{31}P NMR shift

2.2.1. Models for alumina surface sites

To model the adsorption of phosphate on γ-Al_2O_3, we focused on the two predominant (1 1 0) and (1 0 0) facets [34,35,56] built from the non-spinel γ-Al_2O_3 bulk model by Krokidis et al.[57]. Gibbs free energies were calculated within the rigid rotor, harmonic oscillator and ideal gas approximations evaluated from relaxed geometries and electronic structures using periodic density functional theory (DFT) with the PBE-D3 functional[58–60] as implemented in VASP v5.4.1.[61] Chemical shift calculations were done using the GIPAW method using three different aluminum phosphates as reference.[62,63] All computational parameters, references and complementary structures are given in the **Supporting Information S2**. For sake of clarity, we recall in what follows the main key insights regarding the alumina surface models and the nature of exposed Al or Al-OH sites which are mandatory for the fine understanding of the adsorption mechanism. These results were widely discussed in previous works by comparison with infrared or NMR data.[34,35,40,41,63,64]

Both surfaces are covered by a monolayer of water under drying conditions (120°C and 2 kPa vapor pressure) according to *ab initio* thermodynamics.[34,35] It leads to a similar coverage in water for both facets with 8.6 H_2O nm^{-2} on (1 0 0) and 8.9 H_2O nm^{-2} on (1 1 0). In other words, the simulation unit cells of (1 0 0) and (1 1 0) surfaces contain 4 and 6 water molecules respectively; some of these molecules are dissociated thus forming two hydroxyls (OH). The first OH involves one oxygen atom of the alumina lattice labeled μ_2-OH or μ_3-OH and represented in blue in **fig. 3**. The second OH group (with O represented in red in **fig.3**) is

inherited from the former water molecule and is connected to one or two Al atoms, denoted μ_1-OH and μ_2-OH, respectively. Note: a μ_4-O site also exists and is never protonated in stable configurations. The diversity of these O-surface sites have been recently revisited by ^{17}O NMR.[65]

For the (1 1 0) orientation, we also considered the surface reconstruction proposed by Wischert et al.,[64] which consists in a migration of one octahedral aluminum atom (Al_{VI}, see arrow in **fig. 3b**) to a neighbouring tetrahedral site (Al_{IV}, see arrow in **fig. 3c)**. Upon reconstruction, one adsorption site is removed due to the $Al_{VI \rightarrow IV}$ shift (7.4 H_2O nm^{-2}) and one water molecule is desorbed. This surface reconstruction is energetically 29 kJ mol^{-1} less stable than the initial (1 1 0) at working conditions. The resulting reconstructed surface will be referred to as R(1 1 0), while the "normal" unreconstructed surface will be referred to as n(1 1 0).

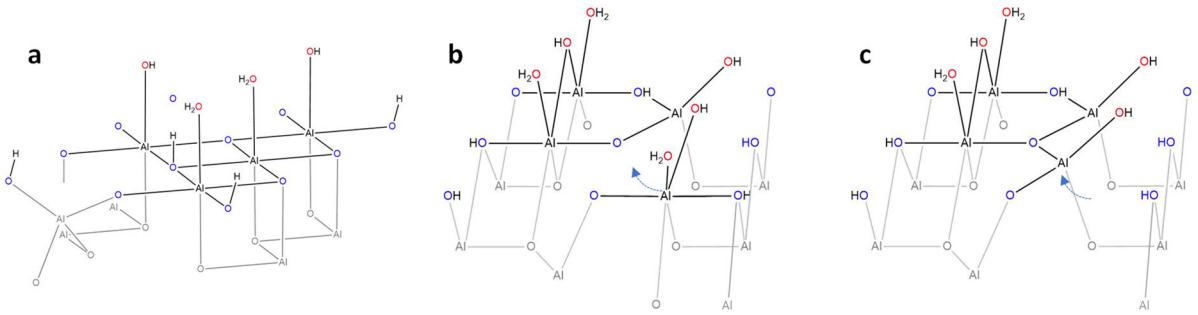

Figure 3: Schematic perspective view of the hydrated γ-Al_2O_3 reference surface structures. Oxygen atoms originating from water adsorbed molecules are shown in red, the ones from the bulk γ-Al_2O_3 are shown in blue. Surface aluminum atoms are shown in black, the subsurface ones in grey. (a) (1 0 0) facet has 4 inequivalent octahedral Al_{VI} exposed for adsorption, which can accept one H_2O molecule each; (b) the n(1 1 0) facet exposes 3 inequivalent octahedral Al_{VI} and 1 tetrahedral Al_{IV} site: Al_{IV} binds one μ_1-OH, the two neighboring Al_{VI} bind to μ_1-OH, μ_1-OH_2 and μ_2-OH and the further Al_{VI} presents two adsorption sites and binds to μ_1-OH and μ_1-OH_2; (c) the reconstructed R(1 1 0) facet results from the migration of one Al_{VI} to an Al_{IV} site (represented by the arrows), which induces the loss of one chemisorbed water, the transformation of a μ_3-OH into a μ_2-OH, and some proton rearrangements.

Considering the hydration state of the surfaces, these models exhibit a great majority of Al_{IV} and Al_{VI} surface sites. Previous works showed a good agreement between calculated ^{27}Al chemical shift on similar surface models and experimental NMR value, whatever the hydroxylation state.[63] According to the hydroxylation state considered here (close to dried conditions), the surface does not exhibit Al_V by construction. However, the last water molecules adsorbed on Al_{VI} sites located on the (100) and (110) surfaces are rather weakly bonded[34,35,56] and their stability is rather sensitive to small variations of working conditions explaining the observation of a minority of Al_V sites by NMR in absence[67] or in presence of P-adsorbed species (as shown before).

2.2.2. Adsorption mechanisms

We assume here that the adsorbed state of phosphates is inherited from the drying process and conditions, which were accounted for by the corresponding thermal and pressure corrections in the evaluation of the free enthalpy of these systems (see **Supporting Information 2**). Upon phosphate adsorption a certain amount y of protons (y, see below) might be transferred to the surface forming adsorbed hydroxyls (*OH) or water ($*H_2O$), where * indicates adsorbed moieties (**fig. 4**). Moreover, as phosphate substitutes one or more $*H_2O$ or $*OH$, x water molecules are released into the gas phase. We thus obtain the following general equation, using the (1 0 0) and n(1 1 0) facets shown in **fig. 3a** and **fig. 3b** as an energy reference:

$$H_3PO_4 + (x–y)\ *H_2O + y\ *OH \rightarrow *H_{3-y}PO_4 + x\ H_2O \quad (1)$$

On the (1 0 0) and n(1 1 0), the dentation mode, denoted as ν_x, of the adsorbed phosphate is directly related to x, the number of released water molecules. It can vary from physisorbed (ν_0) to tridentate (ν_3) with three (P)-O-Al bonds (see **fig. 4**). Constructing monodentates ν_1 and bidentates ν_2 is possible by substitution of sites defined by preadsorbed water (red-highlighted oxygens in **fig. 3**). Tridentates ν_3 are only possible by binding three phosphate oxygens that are

arranged as a near-regular triangle with a side length of about 2.6 Å. To reach this optimal configuration, the H_3PO_4 chemisorption involves the substitution of one oxygen atom of H_3PO_4 by one oxygen atom of the first alumina layer (blue-highlighted oxygen atoms in **fig. 3**). Then, one of the *x* water molecules that are released originates from the dehydration of H_3PO_4. This means for tridentates (ν_3) that the *x* released H_2O are not only related with the number of H_2O in the preadsorbed water monolayer. As exception, this can be avoided in one case on the (1 0 0) facet, by considering a right triangle of 3 preadsorbed water – at the cost of significant structural distortion.

In our configuration screening of H_3PO_4 adsorption, we also considered the reconstruction of the n(1 1 0) surface into the R(1 1 0) surface. As explained above, it is associated with the desorption of a water molecule:

$$\mathbf{[n]} \rightarrow \mathbf{[R]} + H_2O \qquad (2)$$

with **[n]** the unreconstructed reference structure and **[R]** the reconstructed reference structure shown in **fig. 3b** and **c** respectively. Then, for this particular case, (1) is modified accordingly, with the release of $x+1$ water molecules upon adsorption in a dentation mode ν_x:

$$H_3PO_4 + (x-y)\ \mathbf{[n]}^*\ H_2O + y\ \mathbf{[n]}^*OH \rightarrow \mathbf{[R]}^*H_{3-y}PO_4 + (x+1)\ H_2O \qquad (3)$$

In total, we have screened more than 1000 configurations encompassing (i) the four adsorption modes ν_x (see **fig. 4**) (ii) all possible sites on the three studied surface models: (1 0 0), n(1 1 0) and R(1 1 0) (iii) co-adsorbed monophosphates and diphosphate adsorption by combining all possible pairs of ν_x modes in the two monophosphate fragments of their parent co-adsorbed model. The description procedure and the full list of the most stable adsorption for each site and adsorption mode is given in **Supporting Information 2.2**.

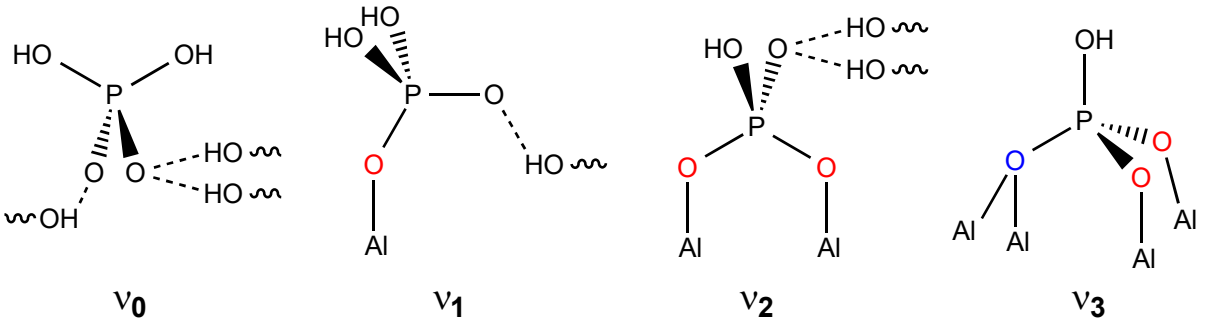

Figure 4: The four possible adsorption modes of chemisorbed phosphoric acid on γ-Al_2O_3: from no phosphoric acid O atoms bonded to alumina Al atoms (ν_0) to three O atoms bonded to the surface Al atoms (ν_3). Chemisorbed hydroxyls –OH and water –H_2O are represented interchangeably in black by OH groups with wiggle bonds. H-bonds with neighboring OH and H_2O are symbolized by dashed lines. O-Al bonds represent bonds to the surface Al atoms. Phosphate oxygen atoms substituting chemisorbed water are represented in red, one oxygen atom belonging to the alumina network is shown in blue.

2.2.3. Mono-Phosphate adsorption

The four adsorption modes, ν_0, ν_1, ν_2, and ν_3, of $*H_{3-y}PO_4$ on the three surface models (1 0 0), n(1 1 0) and R(1 1 0), correspond to 12 most favorable configurations. Their calculated free enthalpies of adsorption ΔG_{ads} and ^{31}P-NMR chemical shifts are reported in **fig. 5**. Our systems represent surface coverages of 1.5 and 2.2 P nm^{-2} for the (1 1 0) and (1 0 0) facets, respectively. The consistency of the results presented below was also checked for the most favorable configurations at lower coverages: 0.7 P nm^{-2} on the (1 1 0) and 1.1 P nm^{-2} on the (1 0 0) surface (see **Supporting Information 3.2**) which correspond to the lowest coverages studied in NMR. This complementary analysis shows that the trend at lower coverages remains unchanged.

In the experimentally relevant chemical shift range of 0 to -20 ppm, we mainly find bidentates (ν_2) and tridentates (ν_3) adsorbed on the (1 1 0) facets. Interestingly, many of those configurations are also the most stable ones, matching with the experimental data in the low coverage regime. Notably, on the lowest chemical shift range (-10 ppm to -20 ppm), we find

two n(1 1 0) adsorption modes. The reconstruction stabilizes the adsorption and leads to a change in chemical shift of about +10 ppm with a chemical shift between 0 ppm and -10 ppm. The ν_3 mode on R(1 1 0) is the most stable system, followed by ν_2 on R(1 1 0), both being more stable than the corresponding adsorptions on the n(1 1 0) by at least 17 kJ.mol^{-1}. This can be related to phosphate condensation with an alumina μ_2-OH generated by the n→R surface reconstruction (**fig. 5b**), which would otherwise be unlikely as these hydroxo groups are the least prone to bind to other species according to Ref.[66] This condensation also occurs on the n(1 1 0) surface to stabilize the tridentate ν_3 but the alumina μ_3-OH is less active. By contrast, the adsorption configurations on the (1 0 0) surface reveal all high (positive) chemical shifts including the most stable ν_2 configuration.

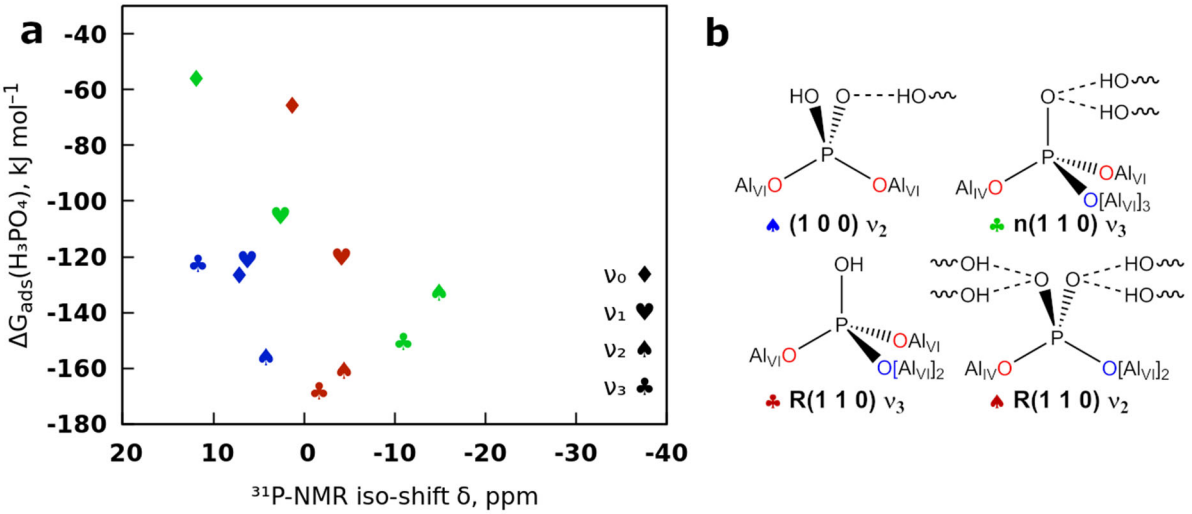

Figure 5: (*a*) Computed ^{31}P NMR chemical shifts vs. Gibb's free adsorption enthalpies of single monomers on the n(1 1 0) (green symbols), R(1 1 0) (deep red symbols) and (1 0 0) (blue symbols) facets (1.5 and 2.2 P nm^{-2} respectively). The n(1 1 0) and R(1 1 0) share the same energetic reference in Gibbs Free enthalpy computations (see Equation 3). (*b*) Schematic representation of the four most stable configurations. Phosphate oxygen atoms substituting chemisorbed water are represented in red, one oxygen atom belonging to the alumina network is shown in blue.

2.2.4. Mono-Phosphate co-adsorption

To describe higher coverages as explored by NMR experiments, another phosphate monomer was added in the simulation cell to obtain 4.3 P nm^{-2} on the (1 0 0) facet and 3.0 P nm^{-2} on both (1 1 0) facets. For comparison with the previous section, we express ΔG_{ads} per mole of phosphate and use a generalized notation for the dentation modes "ν_a+ν_b" for the co-adsorption of phosphate ν_a with phosphate ν_b (see also **Supporting Information 2.2**). As our results for single phosphate adsorption showed that ν_0 and ν_1 are significantly less stable, we only show adsorption modes involving at least one bidentate or tridentate adsorption mode (see **fig. 6a**). For the most stable ones, we determined the ^{31}P-NMR chemical shifts of each ^{31}P nucleus, thus giving two shifts per configuration. **Fig. 6a** plots ΔG_{ads} as a function of ^{31}P-NMR shift for those cases.

The main trends are similar to the single phosphate adsorption case, but the chemical shift range is slightly broadened in comparison with single phosphate adsorption. Adsorption on the (1 0 0) facet still tends to push the ^{31}P-NMR chemical shift above 0 ppm and to be less favored than on the (1 1 0) facet. The most favorable configuration R(1 1 0) ν_2+ν_1 leads to chemical shifts of -5.1 and +2.2 ppm while n(1 1 0) ν_3+ν_2 and ν_2+ν_2 lead to lower chemical shifts (in the -9 to -13 ppm range), closer to the ones observed at a lower coverage (**Fig. 5a**). Noticeably, the highest dentation ν_3+ν_3 is sterically hindered and therefore is not anymore the most stable adsorption mode.

Note that R(1 1 0) ν_2+ν_1 keeps involving the μ_2-OH group generated upon surface reconstruction (see **fig. 6b**). Since this μ_2-OH site is unique in the cell, it can only stabilize one phosphate. Moreover, as R(1 1 0) ν_2+ν_1 is only 5 kJ mol^{-1} more stable than the two most stable adsorption modes on n(1 1 0), we should therefore expect the unreconstructed system to

account for at least a relatively small fraction of the various structures compatible with experimental data (at 120 °C the Boltzmann population ratio between the two systems is 0.22, indicating that they should co-exist at these conditions).

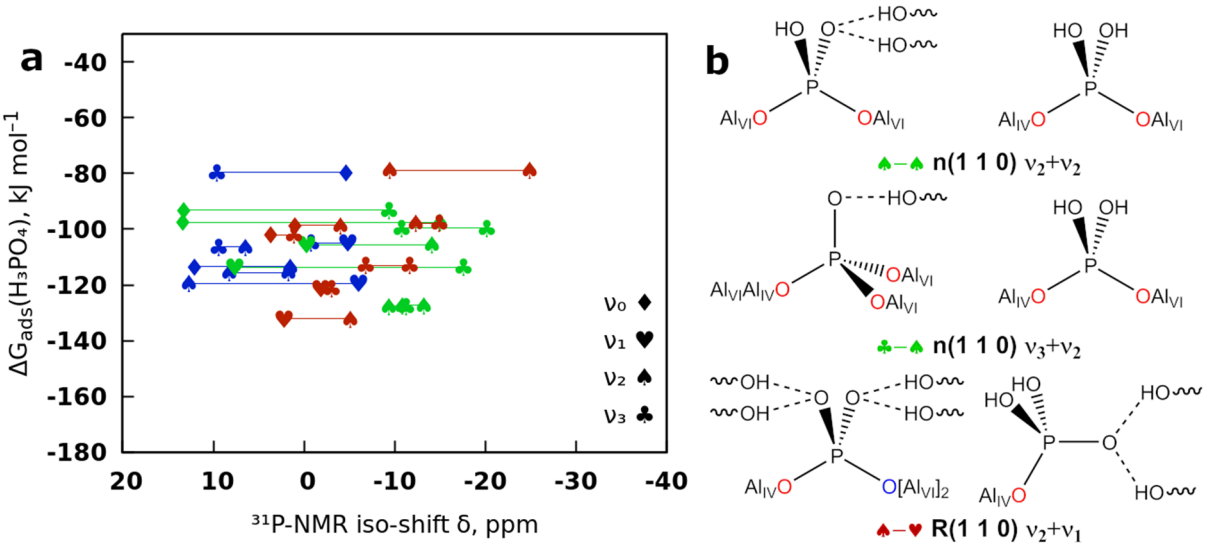

Figure 6: (a) Computed ^{31}P-NMR chemical shifts of co-adsorbed monomers vs. Gibb's free adsorption enthalpies (in kJ mol^{-1} of 1 phosphate) on the n(1 1 0) (green symbols), R(1 1 0) (deep red symbols) and (1 0 0) (blue symbols) facets. The n(1 1 0) and R(1 1 0) share the same reference Gibbs free enthalpy (see Equation 3). Coverages are 3.0 and 4.3 P/nm^2 for the (1 1 0) and (1 0 0) facets, respectively. Each configuration produces two phosphates NMR signals represented by two connected symbols. Only systems with one ν_2 or ν_3 monomer are shown. (b) Schematic representation of the three most stable configurations. Phosphate oxygen atoms substituting chemisorbed water are represented in red, one oxygen atom belonging to the alumina network is shown in blue.

2.2.5. Phosphate dimer adsorption

To explore the stability of phosphate oligomers on the surface, we simulated diphosphate adsorption at the same coverage as co-adsorbed phosphates (3.0 and 4.3 P/nm^2) and determined the ^{31}P-NMR chemical shifts of each ^{31}P nucleus of the most stable configurations. The

formation of a diphosphate induces the condensation reaction of phosphate acid thus releasing half a water molecule per phosphate unit:

$$H_3PO_4 \rightarrow \frac{1}{2} H_4P_2O_7 + \frac{1}{2} H_2O \quad (4)$$

Using eq. 4 and eq. 2 (twice) we can derive for the oligomerizing adsorption over (1 0 0) and n(1 1 0):

$$2\ H_3PO_4 + (x\text{-}y)\ {*}H_2O + y\ {*}OH \rightarrow {*}H_{4-y}P_2O_7 + (x+1)\ H_2O \quad (5)$$

Here, x denotes the sum of the phosphate dentations. Hence, the diphosphate adsorption modes will be denoted as ν_{ab}, a and b corresponding to the adsorption mode of each individual phosphate group and $a+b = x$. The resulting ΔG_{ads} is provided per mole of phosphate and plotted as a function of ^{31}P-NMR chemical shift in **fig. 7a** for the cases analogous to the ones investigated in co-adsorption.

Generally, there are much fewer possibilities to arrange the diphosphates on the surface sites than to co-adsorb two monophosphates. The structural patterns of those chemisorbed diphosphates are inherited from monophosphate adsorption, but their relative stability can differ. The most stable adsorbed diphosphates, R(1 1 0) ν_{31} and R(1 1 0) ν_{22}, still benefit from the condensation with the μ_2-OH site formed upon surface reconstruction during the adsorption of R(1 1 0) ν_3 and R(1 1 0) ν_2 modes as shown in **fig. 7b**. It yields a strong stabilization of the (1 1 0) reconstruction since R(1 1 0) ν_{31} is 20 kJ mol^{-1} more stable than the best configuration ν_{21} on n(1 1 0). This stabilization is much stronger than the one found for co-adsorbed monomers. On the (1 0 0) facet, the ν_{21} mode is the most stable dimer and it is 11 kJ mol^{-1} higher in energy than R(1 1 0)ν_{31}. In terms of ^{31}P NMR chemical shift calculations, oligomers are found in a significantly more negative range than the monomers, between about –10 and –30 ppm, the most stable systems on (1 0 0) producing a signal at its upper end.

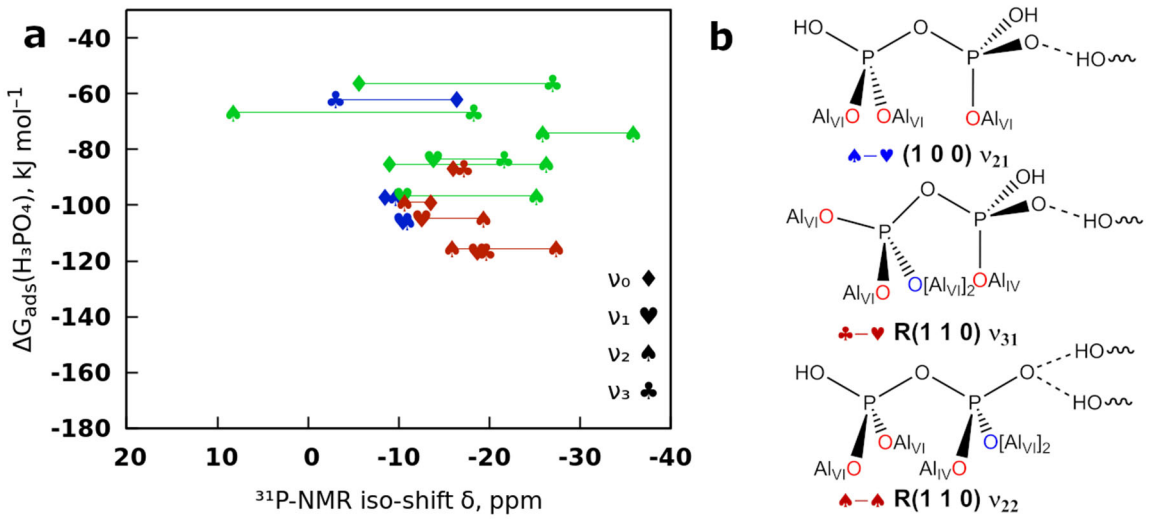

Figure 7: (a) Computed ^{31}P-NMR chemical shifts of the dimer as the most significant polyphosphate, $H_4P_2O_7$ adsorption modes on the different facets vs. Gibb's free adsorption enthalpies (in kJ mol^{-1} phosphate) on the n(1 1 0) (green symbols), R(1 1 0) (deep red symbols) and (1 0 0) (blue symbols) facets. The n(1 1 0) and R(1 1 0) share the same reference Gibbs free enthalpy (see Equation 3). Coverages are 3.0 and 4.3 P/nm^2 for the (1 1 0) and (1 0 0) facets, respectively. Each configuration produces two phosphates NMR signals represented by two connected symbols. Full symbols: phosphate in the same configuration (mode and site) as in **fig. 5**; hollow symbols: phosphate in a new configuration. (b) Schematic representation of the three most stable configurations. Phosphate oxygen atoms substituting chemisorbed water are represented in red, one oxygen atom belonging to the alumina network is shown in blue.

2.2.6. H_3PO_4 adsorption energy trends under drying conditions

The general evolution of the Gibbs free enthalpy of H_3PO_4 adsorption (ΔG_{ads}) with different modes and coverages is linked to H_2O desorption. During phosphate adsorption, the water desorption is directly related to (i) the phosphate dentation with the release of *x* water molecules for a *x*-dentate adsorption mode (see Eq. 2), (ii) the oligomerisation – with the release of 1 extra water molecule (Eq. 5) and (iii) the (1 1 0) reconstruction – with the release of 1 water molecule as well (Eq. 3). **Fig. 8** presents ΔG_{ads} as function of the number of desorbed H_2O molecules for the most stable adsorption mode of H_3PO_4 at a given coverage in order to better assess the

impact of the number of removed water molecules in these energy trends. Similarly, we produced plots for enthalpy ΔH_{ads} and entropy ΔS_{ads}, shown in **fig. S10a** and **b**.

At 120°C and 2 kPa vapor pressure, the most stable system found is R(1 1 0)ν_3, ΔG_{ads} = −167 kJ mol^{-1}. It is followed by (1 0 0)ν_2, −156 kJ mol^{-1}. Co-adsorption of two phosphates yields to ΔG_{ads} = −132 kJ mol^{-1} for R(1 1 0)ν_2+ν_1, two iso-energetic modes, n(1 1 0)ν_3+ν_2 and ν_2+ν_2 with ΔG_{ads} = −127 kJ mol^{-1}, and −119 kJ mol^{-1} for (1 0 0)ν_2+ν_1. Dimers are the least stable group with −116 kJ mol^{-1} for R(1 1 0)ν_{31} and −106 kJ mol^{-1} for (1 0 0)ν_{21}. Since dimers are thermodynamically less stable than co-adsorbed monomers, we infer that surface oligomerization is not favorable for the tested coverages. As monomer adsorption is stronger on the (1 1 0) surface, this surface will be the first to be covered with phosphates. Since the co-adsorption on the (1 1 0) surface is less favorable than the single adsorption on the (1 0 0) surface for one mole of phosphate, the (1 0 0) will be gradually covered as the content of P increases and before full coverage on (1 1 0) is reached. With respect to dentation modes, the most stable ones are ν_2 and ν_3 on both facets, at coverages presenting monomer adsorption. As P coverage increases, the likelihood of ν_3 modes diminishes in favor of ν_2.

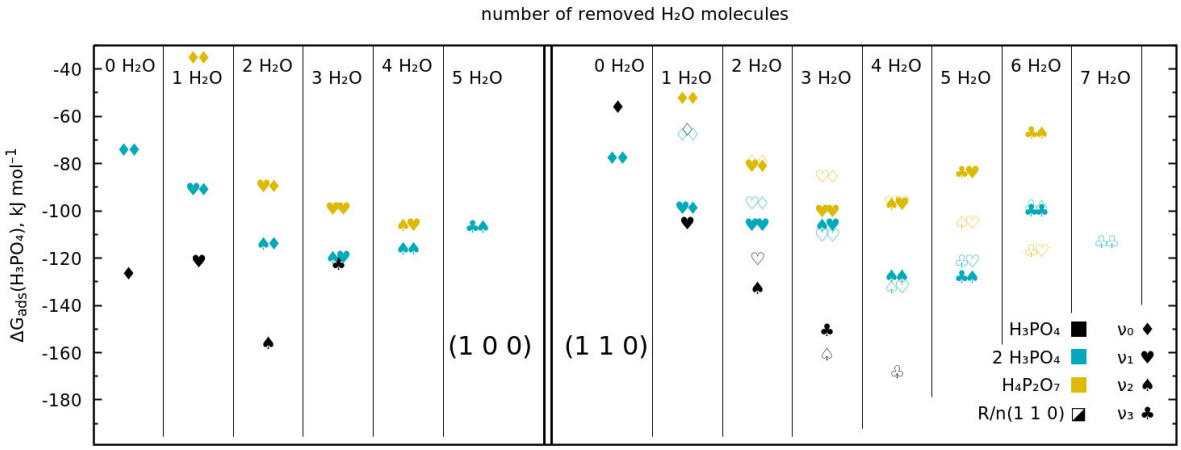

Figure 8: Gibbs free enthalpy of H_3PO_4 adsorption per mole of phosphate as a function of the number of released water molecules from the reference surfaces. For R(1 1 0), the common energy reference of the n(1 1 0) surface was used, hence adsorption occurs after removal of 1 H_2O. Only the lowest enthalpy system of each category is included. Left panel: adsorption on

the (1 0 0) surface; Right panel: adsorption on the (1 1 0) surfaces, n(1 1 0) with filled symbols, R(1 1 0) with empty symbols.

For a better rationale of these observations, the contributions of enthalpy, ΔH_{ads}, and entropy terms, $-T\Delta S_{ads}$, to ΔG_{ads} need to be disentangled. One key aspect is the total number of water molecules that desorb under drying conditions. Both ΔH_{ads} and $-T\Delta S_{ads}$ are linearly correlated with respect to the number of removed water molecules over a larger energy range, but with an opposite slope (see **fig. S10a** and **b**). Each water desorption yields to a 76 kJ mol^{-1} entropy gain (at T= 120 °C). This gain is counterbalanced by an enthalpy change, which is due to the loss of Al-OH_n and H-bonds, in the reference surface, that are only partly compensated in the final state by the formation of Al-O(P) bonds and by the rearrangement of the H-bond network. Higher dentations are accompanied by removal of more water and hence are favored entropically, up to a point where the enthalpy change of the reaction becomes endothermic and too large to be compensated by the entropy gain. The turning point depends on site distortions and proton affinity of the facet. For instance, from (1 0 0)ν_2 to (1 0 0)ν_3 we observe a strong destabilization as the tridentate on this facet introduces a major distortion. Moreover, the maximum allowed number of water removal for the (1 1 0) surface is 7 H_2O, but we already observe a positive enthalpy change from 4 H_2O. We could therefore suggest that the rationale of this behavior is the overall decrease of protons necessary for stabilizing the surface H-bond network.

Since entropy is one key ingredient controlling the dentation, the drying temperature, or more generally speaking the thermal treatment, is expected to change the dentation mode. When dropping to room temperature, the entropic gain per water decreases to 58 kJ mol^{-1}. On the (1 0 0), the most stable adsorption mode shifts from ν_2 to ν_0, (see tab. S6). The energy difference between the n(1 1 0) and the reconstructed surface R(1 1 0) narrows, but the most stable adsorption mode remains on R(1 1 0) with a dentation of ν_2. On the other hand, the thermal

treatment can also be performed at a higher temperature. On (1 1 0), the highest dentation of two phosphates, R(1 1 0)ν_3+ν_3 (involving the release of 7 H_2O), is the most stable system above 200°C. To favor tridentates (ν_3) on (1 0 0), the thermal treatment must be raised beyond 300°C. At such high temperature, phosphates (see fig. 9) bind more deeply into the alumina through a condensation reaction with μ_2-OH or μ_3-OH sites. This adsorption mode can be seen as a potential precursor towards an aluminum phosphate phase appearing at high temperature.[7]

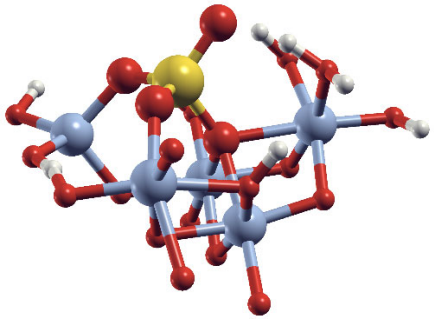

Figure 9: Ball-stick model of n(1 1 0)ν_3. Aluminum, phosphorus, oxygen and hydrogen are colored blue, yellow, red and white, respectively. Phosphate oxygens were increased in size as a guide to the eye.

3. DISCUSSION

In this section we try to infer the influence of surface P coverages on the speciation and the nature of the adsorbed species by comparing our results from NMR spectroscopy and DFT calculations. NMR provides clear evidence for phosphate oligomers at coverage as low as 1 P nm^{-2}. The oligomerization can either occur in solution (eq. 4) or take place after adsorption on the surface (eq. 5). Indeed, earlier experimental studies showed that in solutions heated to 120 °C, among 10 % of phosphate are biphosphate, with traces of triphosphate.[67] Other experiments also showed that the oligomerization and hydrolysis of phosphates can be both catalyzed on mineral surfaces with the drying process being a key factor.[68] Keeping this in mind, we split the discussion into low and high coverage regimes.

3.1. At low coverage (0.4 – 2 P nm^{-2})

The DFT results of single phosphate adsorption (**fig. 5**) indicate that the adsorption of monophosphates with covalent bonds is predominant at low coverage. For all types of surfaces, non-covalent physisorption (ν_0) is less stable and exhibits too-high chemical shifts with respect to the experiments (**fig. 1**). Through-bond ^{27}Al-^{31}P correlation experiments (**fig. 2**) confirm that Al–O–P chemical bonds form, including at the lowest coverage investigated here. This indicates that in this low coverage regime, monophosphates are chemisorbed on the alumina surfaces.

Monophosphate covalently bonded on the (1 1 0) facet stabilizes the reconstruction of this surface through condensation with the generated μ_2-OH groups in R(1 1 0)ν_2 (initially μ_3-OH before surface reconstruction) and R(1 1 0)ν_3. Their predicted ^{31}P NMR chemical shifts values of -4.4 and -1.7 ppm, are compatible with the experimental range. Moreover, the Al sites of the (1 1 0) surface involved in the most relevant adsorption modes are Al_{IV} and Al_{VI}, which agrees with ^{27}Al-^{31}P through-bond INEPT experiments (**fig. 2**). As a tendency, in the INEPT spectra, the through-bond P-O-Al_{VI} correlations are more intense than the P-O-Al_{IV} correlations (**fig. S4b**) , in line with the higher proportion of Al_{VI} sites overall involved in R(1 1 0)ν_2 and R(1 1 0)ν_3. In contrast, adsorption on the (1 0 0) surface is less stable than on the (1 1 0) surface and since it involves Al_{VI} sites only, it cannot alone account for the Al_{IV} sites observed experimentally. In addition, the predicted ^{31}P NMR chemical shifts on the (1 0 0) surface are not compatible with the observed experimental range.

One-dimensional ^{31}P through-bond double- and triple-quantum filtered experiments clearly show the presence of biphosphates at coverages of 1 and 2 P nm^{-2}, and of higher oligomers at 2 P nm^{-2} (**fig.1**). On the other hand, our DFT Gibbs Free energies indicate that the oligomerization on the alumina surface is unlikely since dimers are less stable than co-adsorbed monomers (see **fig. 8**). Therefore, dimers or oligomers covalently bonded to the surface should result from the direct adsorption of dimers or oligomers initially present in solution.[67] The

computed ^{31}P NMR chemical shifts of dimers on the (1 0 0) surface such as ν_{21} are -11 to -10.4 ppm (**fig. 7**), i.e. they are shifted to lower values with respect to monophosphates, which corresponds relatively well to the experimental values (green and purple traces in **fig. 1b**). By contrast, the predicted chemical shifts of dimers covalently bonded to the R(110) surface are more strongly shifted, namely in the range between -16 and -27 ppm, i.e. towards more negative values than those observed experimentally in the refocused INADEQUATE spectra (**fig. 1**). Hence, dimers are covalently bonded on the (1 0 0) surface mainly. We note here that the INADEQUATE spectra display a very broad resonance the tail of which extends down to -30 ppm. This lowest shift region would correspond to the signal of central P atoms of larger oligomers, as indicated by the triple-quantum filtered spectrum of the 2.0 P nm^{-2} loaded alumina (purple traces in fig. 1c).

3.2. At high coverage (greater than 2 P nm^{-2})

At coverage above 2 P nm^{-2}, the ^{27}Al-^{31}P INEPT experiments reveal that through-bond correlation between P and Al_{IV} or Al_{VI} are present in all samples (**fig. 2**), which is consistent with calculated co-adsorption structures (**fig. 6 b**). Since the most stable DFT structures are still favored on the (1 1 0) facet, this is the facet on which covalently bonded P species are predominant and involve Al_{IV} and Al_{VI} sites. **Supporting Information S3.3** reports the calculated ^{27}Al δ_{iso} corresponding to the Al_{IV} and Al_{VI} sites which are either covalently or non-covalently bonded to P through Al-O-P. As revealed by INEPT experiments (**Tables S3 and S4**), we observe an increasing upfield shift of ^{27}Al covalently or non-covalently bonded to P through P-O-Al bridge with increasing P coverage. Similarly, DFT calculations show that the presence of adsorbed phosphorus species induces an upfield shift of ^{27}Al δ_{iso} for Al sites in close vicinity of P and it is generally all the more pronounced as the P coverage increases (**Figure S11**). This interesting surface phenomenon may be compared to the one reported for

aluminophosphate species in solution where the complexation of hexacoordinated Al by phosphates induces a shift of -7.5 to -9 ppm with respect to hexaaquaaluminum cation.[69,70] Even if further analysis might be necessary to better quantify this phenomenon, we may already propose that the presence of phosphates and polyphosphates would increase the shielding of Al sites which are covalently bonded or located in close vicinity to P. As a corollary, two-dimensional ^{31}P-^{27}Al dipolar INEPT experiments is a powerful technique to highlight this fine effect occurring on the P-alumina surface.

The experimental average ^{31}P NMR chemical shift is continuously broadened and displaced towards more negative values with the increase of the P content over γ-Al_2O_3 (**fig. 1**). The experimentally observed shift to lower ppm can be related to the enhanced contribution of $n(1\ 1\ 0)\nu_3+\nu_2$ (-11.3 and -9.4 ppm) and $\nu_2+\nu_2$ (-13.2 and -10.9 ppm) with respect to the slightly more stable $R(1\ 1\ 0)\nu_2+\nu_1$ (-5.1 ppm and 2.2 ppm). Interestingly, aluminophosphate complexes in solution may exhibit ^{31}P chemical shift of -13 ppm.[69,70] Moreover, we observe that co-adsorbed bidentates are significantly more stable than tridentates (**fig. 8**), and that they also occur in a lower ppm range than them (**fig. 5**).

However, these co-adsorbed monomers do not account for the larger chemical shifts observed neither in INADEQUATE nor in INEPT experiments. At coverage greater than 2 P nm^{-2}, dimers and other oligomers are clearly observed in ^{31}P double- and triple-quantum filtered spectra (**fig. 1**). Moreover, at a coverage of 4.1 P nm^{-2}, scalar-based INEPT and INADEQUATE spectra are very similar with a common resonance signal centered at around -18 ppm (**fig. S6)**. Hence, the low ppm range demands a different rationale, involving an increasing surface concentration of oligomers with an increasing P coverage. First, the increase of P surface concentration reduces the surface coverage in water during phosphate deposition, which hampers the available "active" sites of surface hydrolysis of oligomers originating from the solution,[67] thus preserving

covalently-bonded oligomers of ν_{xy} type (with $x,y > 0$). The decrease of hydroxyl coverage during phosphate exchange is also reported by various infrared spectroscopy studies.[7,23,24]

Limiting the hydrolysis of oligomers coming from the solution increases the oligomer surface concentration. For instance, the formation of ν_{x0} species from ν_{00} one is an exergonic process (**Table S8**). Then, increasing further the P concentration (beyond 3.0 P nm^{-2}) leads to a full saturation of the surface aluminum sites. In this regime, the further increase of covalently bonded oligomers could be induced by the grafting of monomers or oligomers on monophosphate or oligophosphate already bonded to alumina, through a process like $\nu_2+\nu_0 \rightarrow \nu_{20}$ which is isergonic at 120°C, and thus requires high P concentration.

In summary, covalently bonded (ν_{xy} with $x,y>0$) dimers are thus expected on R(1 1 0) but also a smaller fraction on (1 0 0) as found for low coverage (**fig. 7**). For instance, the predicted chemical shifts for the stable R(1 1 0)ν_{31} are found at -19.7 and -18.7 ppm which correspond well to the common resonance centered at around -18 ppm in 1D ^{31}P INADEQUATE and scalar-based INEPT spectra. Such dimers adsorbed on the R(1 1 0) can therefore contribute to the signals at increasingly negative chemical shifts observed in the NMR experiments. The dipolar-based INEPT spectra show an almost constant upper shift by about +5 ppm with respect to the scalar-based one (**fig. S2)** for all coverages. This trend can be explained by the presence of oligomers of type ν_{x0} on R(1 1 0) where the calculated ^{31}P chemical shifts of the ν_0 phosphate species are found at higher values (-10.6 ppm to -17.2 ppm, **see Table S8).** We note that oligomers of higher number of phosphates that were made visible in the 3Q filtered experiments, add to the signal intensity at chemical shifts even lower than -30 ppm.

3.3 Possible implications for the catalytic active phase

As underlined in Introduction, the nature of covalently or non-covalently bonded species may directly impact the interaction of metallic active phase precursor on γ–alumina surfaces.[5–7,9,12–14,24] In particular, the presence of phosphate covalently bonded to alumina is expected to tune the interaction with the metallic active phase. On the one hand, the metallic precursor may interact through M-O-P-O-Al bridges instead of M-O-Al which will modify the dispersion of the metallic phase on the support. Depending on the relative strength of M-O-P vs M-O-Al bridges, the dispersion and stability of the metallic phase might be enhanced or diminished by the presence of phosphorus. Simultaneously, the mechanisms of reduction or sulfo-reduction of the metallic active phase which involves breaking such Mo-O-P or Mo-O-Al bond breaking will also depend on the strength of those chemical bridges. According to our DFT calculations, the (110) and (100) surfaces exhibit different behavior with respect to phosphates interaction: the (110) exhibit a higher stability for covalently bonded phosphates, while the (100) would favor non covalently bonded phosphates. This would imply that the interaction of the active phase precursors should depend on the type of facets exposed by alumina. Such a heterogenous behavior of facets has been highlighted by means of model surfaces on α–alumina single crystals.[12] This trend will have important impact for the resulting catalyst, because it means that the concentration of phosphorus should also be optimized as a function of the morphologies of the γ–alumina platelets (not only its overall specific surface area).

Moreover, our work highlights the presence of polyphosphates either covalently or non-covalently bonded to alumina. The presence of such covalently bonded phosphate oligomers may even further influence the genesis of the active phase, while polyphosphates forming more extended patches (either covalently o non covalently bonded) may also imply a more inhomogeneous distribution of the active phase by steric hinderance of the genesis mechanisms.

4. CONCLUSIONS

Adding phosphorous is central to obtain good performance of some heterogeneous catalysts supported over alumina. To unravel the role of P on the catalytic phase morphology and activity, it is necessary to identify the speciation of P species on alumina in function of the surface and the coverage. To do so, we have applied DNP enhanced solid-state NMR spectroscopy to obtain new structural insights into the adsorption modes of phosphates on γ-Al_2O_3. To rationalize the interpretation of the experimental results and a get a full atomic-scale description, we simultaneously explored the stability of phosphate monomers and dimers by DFT calculations on the predominant (1 1 0) and (1 0 0) facets of γ-Al_2O_3. The ^{31}P NMR chemical shifts of the most favorable phosphates among either covalently or non-covalently bonded species were determined and compared with the experimentally observed ^{31}P NMR resonances.

The ^{31}P multiple-quantum filtered 1D spectra as well as the ^{27}Al-^{31}P 2D correlation spectra show that the ^{31}P chemical shifts evolved towards more negative values with increasing loading (0.4 to 4.1 P nm^{-2}), strongly indicating the existence of covalently bonded oligophosphates as confirmed by the calculated DFT ^{31}P chemical shifts of dimers covalently bonded to the (110) surface. Through-bond double-quantum and triple-quantum filtered experiments unequivocally demonstrated for the first time the presence of diphosphates, and tri- or longer polyphosphates which are covalently bonded to the surface, starting from coverage as low as 1 P nm^{-2}. The relative fraction of polyphosphates increases with the P content with a factor 3.5 from the lowest (1 P nm^{-2}) to the highest (4.1 P nm^{-2}) coverage. Thus, the gradual change of the ^{31}P chemical shifts with increasing coverage can be related to the increasing concentration of covalently bonded polyphosphates. According to DFT Gibbs free energies, the hydrolysis of dimers into two monomers is predicted to be exergonic on the γ-Al_2O_3 surfaces. Hence, the observed covalently-bonded polyphosphates result from direct adsorption during impregnation (exergonic process), and eventually at higher concentration from surface oligomerization

(which is at best isergonic). The higher the P coverage, the less likely is the hydrolysis process since this process will be hampered by the lack of available surface sites. In addition, once full saturation of surface sites is reached, the condensation of monomer with pre-adsorbed monomer cannot be excluded. This explains the higher concentration of oligomers at a higher P content.

At low coverage, covalently bonded monophosphates were shown to be intrinsically more stable on the (1 1 0) surface (inducing its reconstruction) than on the (1 0 0) facet, with calculated ^{31}P NMR chemical shifts were found within the range of experimental values. The adsorption of phosphate on the (1 0 0) facet should take place as the P coverage increases.

DNP enhanced ^{27}Al-^{31}P correlation spectra were also recorded, which demonstrate the presence of P-O-Al bonds, preferentially with Al_{VI} and Al_{IV} sites, and to a smaller extent with Al_{V}. INEPT experiments highlighted the shielding effect of adsorbed P on those Al sites. This trend was confirmed by DFT calculations that also revealed that Al_{VI} and Al_{IV} sites of the (1 1 0) surface are involved in the ν_2 and ν_3 covalent bonding modes of mono and diphosphates (with a higher coordination with Al_{VI}). The analysis of the enthalpy and entropy contributions to the Gibbs free enthalpy enabled us to explain the influence of the dentation mode ν_x and of the number of water release from the alumina surface in the energy trends of phosphate adsorption energy. The ν_2 and ν_3 dentations are favored by entropy gain thanks to the release of more water molecules in gas phase.

This deeper understanding offers a rational to control the speciation of P species on alumina, a necessary step towards a better control over the preparation of supported catalysts on this support.

ASSOCIATED CONTENT

AUTHOR INFORMATION

Corresponding Authors

*pascal.raybaud@ifpen.fr

*carine.michel@ens-lyon.fr

*anne.lesage@ens-lyon.fr

Author Contributions

A.H. and D.W. contributed equally. The manuscript was written through contributions of all authors. All authors have given approval to the final version of the manuscript.

Funding Sources

Calculations were performed using HPC resources (Jean Zay and Occigen) from GENCI-CINES (Grant A0020806134) and ENER 440 from IFP Energies nouvelles. This work is part of the "RatiOnAl Design for CATalysis" (ROAD4CAT) industrial chair, project IDEXLYON funded by the French National Research Agency (ANR-16-IDEX-0005) and the Commissariat-General for Investment (CGI) within the framework of Investissements d'Avenir program ("Investment for the future"). The authors thank the SYSPROD project and AXELERA Pôle de Compétitivité for financial support (PSMN Data Center). This work is also supported by the Common Research Laboratory CARMEN (ENS de Lyon, CNRS, IFPEN, Claude Bernard Lyon 1 University, Sorbonne University, and University of Strasbourg).

Supporting Information. Materials and Experimental Methods. Computational details. Complementary results. CIF files of the most relevant structures are also provided.

This material is available free of charge via the Internet at http://pubs.acs.org.

ACKNOWLEDGEMENTS

The authors thank Olivier Ouari (Université Aix-Marseille) for providing the TEKPol radical.

REFERENCES

(1) Bergwerff, J. A.; Visser, T.; Leliveld, B. R. G.; Rossenaar, B. D.; Jong, K. P. de; Weckhuysen, B. M. Envisaging the Physicochemical Processes during the Preparation of Supported Catalysts: Raman Microscopy on the Impregnation of Mo onto Al_2O_3 Extrudates. *J. Am. Chem. Soc.* **2004**, *126*, 14548-14556.

(2) *Catalysis by Transition Metal Sulphides. From Molecular Theory to Industrial Application;* Toulhoat, H.; Raybaud, P., Eds.; Editions Technip: Paris, 2013; pp. 117-223.

(3) van Cleve, T.; Underhill, D.; Rodrigues, M. V.; Sievers, C.; Will Medlin, J. Enhanced Hydrothermal Stability of gamma-Al_2O_3 Catalyst Supports with Alkyl Phosphonate Coatings. *Langmuir* **2018**, *34*, 3619-3625.

(4) R. Iwamoto; J. Grimblot. Influence of Phosphorus on the Properties of Alumina-Based Hydrotreating Catalysts. *Adv. in Catal.* **1999**, *44*, 417-503.

(5) Eijsbouts, S.; van Gestel, J. N. M.; van Veen, J. A.; Beer, V. H. J. de; Prins, R. The Effect of Phosphate on the Hydrodenitrogenation Activity and Selectivity of Alumina-Supported Sulfided Mo, Ni, and Ni-Mo Catalysts. *J. Catal.* **1991**, *131*, 412-432.

(6) Rashidi, F.; Sasaki, T.; Rashidi, A. M.; Nemati Kharat, A.; Jozani, K. J. Ultradeep Hydrodesulfurization of Diesel Fuels Using Highly Efficient Nanoalumina-Supported Catalysts: Impact of Support, Phosphorus, and/or Boron on the Structure and Catalytic Activity. *J. Catal.* **2013**, *299*, 321-335.

(7) Decanio, E. C.; Edwards, J. C.; Scalzo, T. R.; Storm, D. A.; Bruno, J. W. FT-IR and Solid-State NMR Investigation of Phosphorus Promoted Hydrotreating Catalyst Precursors. *J. Catal.* **1991**, *132*, 498-511.

(8) Lewis, J.; Kydd, R. The MoO_3-Al_2O_3 Interaction: Influence of Phosphorus on MoO_3 Impregnation and Reactivity in Thiophene HDS. *J. Catal.* **1992**, *136*, 478-486.

(9) Poulet, O.; Hubaut, R.; Kasztelan, S.; Grimblot, J. Experimental Evidences of the Direct Influence of Phosphorus on Activity and Selectivity of a MoS_2-γAl_2O_3 Hydrotreating Catalyst. *Bull. Soc. Chim. Belges* **1991**, *100*, 857-863.

(10) van Haandel, L.; Bremmer, G. M.; Hensen, E.; Weber, T. The Effect of Organic Additives and Phosphoric Acid on Sulfidation and Activity of (Co)Mo/Al_2O_3 Hydrodesulfurization Catalysts. *J. Catal.* **2017**, *351*, 95-106.

(11) van Haandel, L.; Hensen, E.; Weber, T. High Pressure Flow Reactor for In Situ X-ray Absorption Spectroscopy of Catalysts in Gas-Liquid Mixtures—A Case Study on Gas and Liquid Phase Activation of a Co-Mo/Al_2O_3 Hydrodesulfurization Catalyst. *Catal. Today* **2017**, *292*, 51-57.

(12) Garcia de Castro, R.; Bertrand, J.; Rigaud, B.; Devers, E.; Digne, M.; Lamic-Humblot, A.-F.; Pirngruber, G.; Carrier, X. Surface-Dependent Activation of Model α-Al_2O_3 -Supported P-Doped Hydrotreating Catalysts Prepared by Spin Coating. *Chemistry – A European Journal* **2020**, *26*, 14623-14638.

(13) Ha, K.-S.; Jung, G.-I.; Woo, M.-H.; Jun, K.-W.; Bae, J. W. Effects of Phosphorus and Saccharide on Size, Shape, and Reducibility of Fischer–Tropsch Catalysts for Slurry Phase and Fixed-Bed Reactions. *Appl. Catal. A Gen.* **2013**, *453*, 358-369.

(14) Woo, M. H.; Cho, J. M.; Jun, K.-W.; Lee, Y. J.; Bae, J. W. Thermally Stabilized Cobalt-Based Fischer-Tropsch Catalysts by Phosphorous Modification of Al_2O_3: Effect of Calcination Temperatures on Catalyst Stability. *ChemCatChem* **2015**, *7*, 1460-1469.

(15) Fovanna, T.; Campisi, S.; Villa, A.; Kambolis, A.; Peng, G.; Rentsch, D.; Kröcher, O.; Nachtegaal, M.; Ferri, D. Ruthenium on Phosphorous-Modified Alumina as an Effective and Stable Catalyst for Catalytic Transfer Hydrogenation of Furfural. *RSC Adv.* **2020**, *10*, 11507-11516.

(16) Quartararo, J.; Guelton, M.; Rigole, M.; Amoureux, J.-P.; Fernandez, C.; Grimblot, J. Sol–Gel Synthesis of Alumina Modified by Phosphorus: a Solid State NMR Characterization Study. *J. Mater. Chem.* **1999**, *9*, 2637-2646.

(17) Bergwerff, J. A.; van de Water, Leon G. A.; Visser, T.; Peinder, P. de; Leliveld, B. R. G.; Jong, K. P. de; Weckhuysen, B. M. Spatially Resolved Raman and UV-visible-NIR Spectroscopy on the Preparation of Supported Catalyst Bodies: Controlling the Formation of $H_2PMo_{11}CoO_{405}$− Inside Al_2O_3 Pellets During Impregnation. *Chem-Eur. J.* **2005**, *11*, 4591-4601.

(18) Nicosia, D.; Prins, R. The Effect of Phosphate and Glycol on the Sulfidation Mechanism of CoMo/Al_2O_3 Hydrotreating Catalysts: An in situ QEXAFS study. *J. Catal.* **2005**, *231*, 259-268.

(19) Catita, L.; Quoineaud, A.-A.; Espinat, D.; Pichon, C.; Delpoux, O. Application of Magnetic Resonance Imaging and Raman Imaging to Study the Impact of Phosphorus in Impregnation of Hydrotreatment Catalysts. *Appl. Catal. A Gen.* **2017**, *547*, 164-175.

(20) Zheng, T.-T.; Sun, Z.-X.; Yang, X.-F.; Holmgren, A. Sorption of Phosphate onto Mesoporous γ-alumina Studied with In-Situ ATR-FTIR Spectroscopy. *Chem. Cent. J.* **2012**, *6,* 26, 1-10.

(21) Del Nero, M.; Galindo, C.; Barillon, R.; Halter, E.; Made, B. Surface Reactivity of Alpha-Al_2O_3 and Mechanisms of Phosphate Sorption: In Situ ATR-FTIR Spectroscopy and Zeta Potential Studies. *J. Colloid Interface Sci.* **2010**, *342*, 437-444.

(22) Li, W.; Pierre-Louis, A.-M.; Kwon, K. D.; Kubicki, J. D.; Strongin, D. R.; Phillips, B. L. Molecular Level Investigations of Phosphate Sorption on Corundum (α-Al_2O_3) by ^{31}P Solid State NMR, ATR-FTIR and Quantum Chemical Calculation. *Geochim. Cosmochim. Acta* **2013**, *107*, 252-266.

(23) Roy, T.; Wisser, D.; Rivallan, M.; Catita, L.; Corral Valero, M.; Corre, T.; Delpoux, O.; Pirngruber, G.; Lefèvre, G. Phosphate Adsorption on γ-alumina: A Surface Complex Model Based on Surface Characterization and Zeta Potential Measurements. *J. Phys. Chem. C* **2021**, *125*, 10909-10918.

(24) Lewis, J.; Kydd, R. Adsorption Mechanism of Phosphoric Acid on Gamma-Alumina. *J. Catal.* **1991**, *132*, 465-471.

(25) Johnson, B. B.; Ivanov, A. V.; Antzutkin, O. N.; Forsling, W. ^{31}P Nuclear Magnetic Resonance Study of the Adsorption of Phosphate and Phenyl Phosphates on γ-Al_2O_3. *Langmuir* **2002**, *18*, 1104-1111.

(26) Kim, Y.; Kirkpatrick, R. J. An Investigation of Phosphate Adsorbed on Aluminium Oxyhydroxide and Oxide Phases by Nuclear Magnetic Resonance. *Eur. J. Soil Sci.* **2004**, *55*, 243-251.

(27) van Eck, E. R. H.; Kentgens, A. P. M.; Kraus, H.; Prins, R. A Solid State Double Resonance NMR Investigation of Phosphorus-Impregnated gamma-Al_2O_3. *J. Phys. Chem.* **1995**, *99*, 16080-16086.

(28) Li, W.; Feng, J.; Kwon, K. D.; Kubicki, J. D.; Phillips, B. L. Surface Speciation of Phosphate on Boehmite (gamma-AlOOH) Determined from NMR Spectroscopy. *Langmuir* **2010**, *26*, 4753-4761.

(29) Lesage, A.; Lelli, M.; Gajan, D.; Caporini, M. A.; Vitzthum, V.; Miéville, P.; Alauzun, J.; Roussey, A.; Thieuleux, C.; Mehdi, A.; Bodenhausen, G.; Copéret, C.; Emsley, L. Surface

Enhanced NMR Spectroscopy by Dynamic Nuclear Polarization. *J. Am. Chem. Soc.* **2010**, *132*, 15459-15461.

(30) Kobayashi, T.; Perras, F. A.; Slowing, I. I.; Sadow, A. D.; Pruski, M. Dynamic Nuclear Polarization Solid-State NMR in Heterogeneous Catalysis Research. *ACS Catal.* **2015**, *5*, 7055-7062.

(31) Berruyer, P.; Emsley, L.; Lesage, A. DNP in Materials Science: Touching the Surface. *eMagRes* **2018**, *7*, 93-104.

(32) Hooper, R. W.; Klein, B. A.; Michaelis, V. K. Dynamic Nuclear Polarization (DNP) 101: A New Era for Materials. *Chem. Mater.* **2020**, *32*, 4425-4430.

(33) Corral Valero, M.; Raybaud, P. Computational Chemistry Approaches for the Preparation of Supported Catalysts: Progress and challenges. *J. Catal.* **2020**, *391*, 539-547.

(34) Digne, M.; Sautet, P.; Raybaud, P.; Euzen, P.; Toulhoat, H. Hydroxyl Groups on Gamma-Alumina Surfaces: A DFT Study. *J. Catal.* **2002**, *211*, 1-5.

(35) Digne, M.; Sautet, P.; Raybaud, P.; Euzen, P.; Toulhoat, H. Use of DFT to Achieve a Rational Understanding of Acid-Basic Properties of Gamma-Alumina Surfaces. *J. Catal.* **2004**, *226*, 54-68.

(36) Larmier, K.; Chizallet, C.; Raybaud, P. Tuning the Metal–Support Interaction by Structural Recognition of Cobalt-Based Catalyst Precursors. *Angew. Chem. Int. Ed.* **2015**, *54*, 6824-6827.

(37) Ngouana-Wakou, B. F.; Corral Valero, M.; Raybaud, P. Theoretical Insights Into the Interaction of Oxygenated Organic Molecules and Cobalt(II) precursor with γ-Al_2O_3 Surfaces. *J. Phys. Chem. C* **2018**, *122*, 19560-19574.

(38) Pickard, C. J.; Mauri, F. All-Electron Magnetic Response with Pseudopotentials: NMR chemical shifts. *Phys. Rev. B* **2001**, *63*, 245101.

(39) Charpentier, T. The PAW/GIPAW Approach for Computing NMR Parameters: A New Dimension Added to NMR Study of Solids. *Solid State Nucl. Magn. Reson.* **2011**, *40*, 1-20.

(40) Valla, M.; Rossini, A. J.; Caillot, M.; Chizallet, C.; Raybaud, P.; Digne, M.; Chaumonnot, A.; Lesage, A.; Emsley, L.; van Bokhoven, J. A.; Copéret, C. Atomic Description of the Interface between Silica and Alumina in Aluminosilicates through Dynamic Nuclear Polarization Surface-Enhanced NMR Spectroscopy and First-Principles Calculations. *J. Am. Chem. Soc.* **2015**, *137*, 10710-10719.

(41) Batista, A. T. F.; Wisser, D.; Pigeon, T.; Gajan, D.; Diehl, F.; Rivallan, M.; Catita, L.; Gay, A.-S.; Lesage, A.; Chizallet, C.; Raybaud, P. Beyond gamma-Al_2O_3 Crystallite Surfaces: The Hidden Features of Edges Revealed by Solid-State ^{1}H NMR and DFT Calculations. *J. Catal.* **2019**, *378*, 140-143.

(42) Ashbrook, S. E.; Cutajar, M.; Pickard, C. J.; Walton, R. I.; Wimperis, S. Structure and NMR Assignment in Calcined and As-Synthesized Forms of $AlPO_4$: A Combined Study by First-Principles Calculations and High-Resolution ^{27}Al-^{31}P MAS NMR Correlation. *Phys. Chem. Chem. Phys.* **2008**, *10*, 5754-5764.

(43) Dawson, D. M.; Seymour, V. R.; Ashbrook, S. E. Effects of Extraframework Species on the Structure-Based Prediction of ^{31}P Isotropic Chemical Shifts of Aluminophosphates. *J. Phys. Chem. C* **2017**, *121*, 28065-28076.

(44) Pourpoint, F.; Kolassiba, A.; Gervais, C.; Azaïs, T.; Bonhomme-Coury, L.; Bonhomme, C.; Mauri, F. First Principles Calculations of NMR Parameters in Biocompatible Materials Science: The Case Study of Calcium Phosphates, β- and γ-$Ca(PO_3)_2$. Combination with MAS-J Experiments. *Chem. Mater.* **2007**, *19*, 6367-6369.

(45) Pourpoint, F.; Gervais, C.; Bonhomme-Coury, L.; Azaïs, T.; Coelho, C.; Mauri, F.; Alonso, B.; Babonneau, F.; Bonhomme, C. Calcium Phosphates and Hydroxyapatite: Solid-

State NMR Experiments and First-Principles Calculations. *Appl. Magn. Reson.* **2007**, *32*, 435-457.

(46) Tielens, F.; Gervais, C.; Deroy, G.; Jaber, M.; Stievano, L.; Coelho Diogo, C.; Lambert, J.-F. Characterization of Phosphate Species on Hydrated Anatase TiO_2 Surfaces. *Langmuir* **2016**, *32*, 997-1008.

(47) Zagdoun, A.; Casano, G.; Ouari, O.; Schwarzwälder, M.; Rossini, A. J.; Aussenac, F.; Yulikov, M.; Jeschke, G.; Copéret, C.; Lesage, A.; Tordo, P.; Emsley, L. Large Molecular Weight Nitroxide Biradicals Providing Efficient Dynamic Nuclear Polarization at Temperatures up to 200 K. *J. Am. Chem. Soc.* **2013**, *135*, 12790-12797.

(48) Lesage, A.; Bardet, M.; Emsley, L. Through-Bond Carbon−Carbon Connectivities in Disordered Solids by NMR. *J. Am. Chem. Soc.* **1999**, *121*, 10987-10993.

(49) Cadars, S.; Sein, J.; Duma, L.; Lesage, A.; Pham, T. N.; Baltisberger, J. H.; Brown, S. P.; Emsley, L. The Refocused INADEQUATE MAS NMR Experiment in Multiple Spin-Systems: Interpreting Observed Correlation Peaks and Optimising Lineshapes. *J. Magn. Reson.* **2007**, *188*, 24-34.

(50) Fayon, F.; Roiland, C.; Emsley, L.; Massiot, D. Triple-Quantum Correlation NMR Experiments in Solids Using J-Couplings. *J. Magn. Reson.* **2006**, *179*, 49-57.

(51) Yoza, N.; Ueda, N.; Nakashima, S. pH-Dependence of ^{31}P-NMR Spectroscopic Parameters of Monofluorophosphate, Phosphate, Hypophosphate, Phosphonate, Phosphinate and their Dimers and Trimers. *Fresenius. J. Anal. Chem.* **1994**, *348*, 633-638.

(52) Trebosc, J.; Hu, B.; Amoureux, J. P.; Gan, Z. Through-Space R3-HETCOR Experiments between spin-1/2 and Half-Integer Quadrupolar Nuclei in Solid-State NMR. *J. Magn. Reson.* **2007**, *186*, 220-227.

(53) Amoureux, J. P.; Trebosc, J.; Wiench, J.; Pruski, M. HMQC and Refocused-INEPT Experiments Involving Half-Integer Quadrupolar Nuclei in Solids. *J. Magn. Reson.* **2007**, *184*, 1-14.

(54) Haouas, M.; Taulelle, F.; Martineau, C. Recent Advances in Application of ^{27}Al NMR Spectroscopy to Materials Science. *Prog. Nucl. Magn. Reson. Spectrosc.* **2016**, *94-95*, 11-36.

(55) Viger-Gravel, J.; Paruzzo, F. M.; Cazaux, C.; Jabbour, R.; Leleu, A.; Canini, F.; Florian, P.; Ronzon, F.; Gajan, D.; Lesage, A. Atomic-Scale Description of Interfaces between Antigen and Aluminum-Based Adjuvants Used in Vaccines by Dynamic Nuclear Polarization (DNP) Enhanced NMR Spectroscopy. *Chemistry – A European Journal* **2020**, *26*, 8976-8982.

(56) Euzen, P.; Raybaud, P.; Krokidis, X.; Toulhoat, H.; Le Loarer, J.; Le Loarer, J. L.; Froidefond, C. In *Handbook of Porous Solids*; Schüth, F., Sing, K. S. W., Weitkamp, J., Eds.; Wiley-VCH Verlag GmbH: Weinheim, 2002; pp 1591–1677.

(57) Krokidis, X.; Raybaud, P.; Gobichon, A. E.; Rebours, B.; Euzen, P.; Toulhoat, H. Theoretical Study of the Dehydration Process of Boehmite to gamma-Alumina. *J. Phys. Chem. B* **2001**, *105*, 5121-5130.

(58) Perdew, J. P.; Burke, K.; Ernzerhof, M. Generalized Gradient Approximation Made Simple. *Phys. Rev. Lett.* **1996**, *77*, 3865-3868.

(59) Perdew, J. P.; Burke, K.; Ernzerhof, M. Generalized Gradient Approximation Made Simple [Phys. Rev. Lett. 77, 3865 (1996)]. *Phys. Rev. Lett.* **1997**, *78*, 1396-1396.

(60) Grimme, S.; Antony, J.; Ehrlich, S.; Krieg, H. A Consistent and Accurate Ab Initio Parametrization of Density Functional Dispersion Correction (DFT-D) for the 94 elements H-Pu. *J. Chem. Phys.* **2010**, *132*, 154104.

(61) Kresse, G.; Joubert, J. From Ultrasoft Pseudopotentials to the Projector Augmented-Wave Method. *Phys. Rev. B* **1999**, *59*, 1758-1775.

(62) Yates, J. R.; Pickard, C. J.; Mauri, F. Calculation of NMR chemical shifts for extended systems using ultrasoft pseudopotentials. *Phys. Rev. B* **2007**, *76*, 24401-24412.

(63) Wischert, R.; Florian, P.; Copéret, C.; Massiot, D.; Sautet, P. Visibility of Al Surface Sites of γ-Alumina: A Combined Computational and Experimental Point of View. *J. Phys. Chem. C* **2014**, *118*, 15292-15299.

(64) Wischert, R.; Laurent, P.; Copéret, C.; Delbecq, F.; Sautet, P. γ-Alumina: the Essential and Unexpected Role of Water for the Structure, Stability, and Reactivity of "Defect" Sites. *J. Am. Chem. Soc.* **2012**, *134*, 14430-14449.

(65) Wang, Q.; Li, W.; Hung, I.; Mentink-Vigier, F.; Wang, X.; Qi, G.; Wang, X.; Gan, Z.; Xu, J.; Deng, F. Mapping the Oxygen Structure of γ-Al_2O_3 by High-Field Solid-State NMR Spectroscopy. *Nat. Commun.* **2020**, *11*, 3620.

(66) Corral Valero, M.; Prelot, B.; Lefèvre, G. MUSIC Speciation of γ-Al_2O_3 at the Solid Liquid Interface: How DFT Calculations Can Help with Amorphous and Poorly Crystalline Materials. *Langmuir* **2019**, *35*, 12986-12992.

(67) Thilo, E.; Sauer, R. Zur Chemie der Kondensierten Phosphate und Arsenate. XVII. Der Verlauf und die Produkte der Entwässerung der Monophosphorsäure H_3PO_4. *J. Prakt. Chem.* **1957**, *4*, 324-348.

(68) Georgelin, T.; Jaber, M.; Bazzi, H.; Lambert, J.-F. Formation of Activated Biomolecules by Condensation on Mineral Surfaces: A Comparison of Peptide Bond Formation and Phosphate Condensation. *Orig. Life Evol. Biosph.* **2013**, *43*, 429-443.

(69) Mortlock, R. F.; Bell, A. T.; Radke, C. J. Phosphorus-31 and Aluminum-27 NMR Investigations of Highly Acidic, Aqueous Solutions Containing Aluminum and Phosphorus. *J. Phys. Chem.* **1993**, *97*, 767-774.

(70) Mortlock, R. F.; Bell, A. T.; Radke, C. J. Phosphorus-31 and Aluminum-27 NMR Investigations of the Effects of pH on Aqueous Solutions Containing Aluminum and Phosphorus. *J. Phys. Chem.* **1993**, *97*, 775-782.

FOR TABLE OF CONTENTS ONLY